THE ASTROPHYSICAL JOURNAL, 354:232–241, 1990 May 1

IMAGES OF SHOCK-EXCITED MOLECULAR HYDROGEN IN YOUNG STELLAR OUTFLOWS

ROGNVALD P. GARDEN[1]
Department of Physics, University of California, Irvine

ADRIAN P. G. RUSSELL
Joint Astronomy Center, Hawaii

AND

MICHAEL G. BURTON
Department of Physics, University of California, Irvine, and NASA Ames Research Center
Received 1988 November 17; accepted 1989 November 3

ABSTRACT

We present high-angular resolution molecular hydrogen (H_2) $v = 1$–0 $S(1)$ line images of several well-known molecular outflow sources (DR 21, NGC 2071, HH 7–11, and HH 12). These images were obtained through a 1% narrow-band filter using an InSb infrared detector array with a plate scale of 1.2 arcsec per pixel. It is found that all of the outflow sources possess highly collimated jets of shock-excited gas that are extremely clumpy and often consist of bright knots that are placed periodically along the jet axis. The H_2 emission-line jets are significantly more collimated than their corresponding CO outflows and remain collimated to large distances from their driving source. In DR 21 and NGC 2071, the H_2 jets appear to become more collimated with increasing distance from the central source, suggesting that they are pressure-confined by the ambient cloud medium. In HH 7–11 and HH 12 the shock-excited ionized and molecular components are spatially coincident and appear to be of comparable shape and size; this suggests that the shocked gas is highly mixed on scales significantly smaller than the current spatial resolution ($\sim$0.005 pc at 500 pc). We discuss the shock patterns observed internal to these jets and propose that they are formed by either (i) a varying external pressure, (ii) the growth of shear instabilities along the walls of a pressure-confined jet, or (iii) the collision of a highly collimated wind with numerous preexisting, subsolar mass clumps in the ambient cloud medium.

Subject headings: interstellar: molecules — nebulae: general — shock waves — stars: pre–main-sequence

I. INTRODUCTION

Although the existence of young stellar jets is now firm observational fact, the physical processes responsible for driving and collimating the outflow gas are still poorly understood. The most informative technique for investigating the physical properties of the jets is to obtain images of their line emission at both high-spectral and high-spatial resolution. Although this has been accomplished in several instances, namely for the ionized jets and Herbig Haro objects associated with optically visible T Tauri stars (Mundt, Brugel, and Buhrke 1987; Mundt 1988; Buhrke, Mundt, and Ray 1988), most of the youngest, and hence the most interesting, outflow sources are deeply embedded within the cores of dense molecular clouds and are thus obscured at optical wavelengths. Fortunately, at millimeter wavelengths the cloud medium is usually transparent to line photons, and the kinematics of the outflowing gas can be studied in great detail. However, existing millimeter interferometer arrays, although an improvement over single-dish telescopes, lack the angular resolving power to study in detail the morphology of the outflowing gas and give a poor representation of the large-scale structure. We therefore suggest that the observations of shock-excited line emission in the infrared is probably the best method currently available for studying extended high-velocity molecular outflows at high-angular resolution. This is because at infrared wavelengths the effect of foreground extinction on the emergent radiation is considerably less important than in the visible and also, as a result of the recent introduction of sensitive two-dimensional detector arrays (Wynn-Williams & Becklin 1987), it is now possible to image large areas of the sky in the infrared at arcsec resolution. The most promising near-infrared line to observe is the $v = 1$–0 $S(1)$ transition of molecular hydrogen (H_2) at 2.122 μm. As this line is an excellent tracer of shocked gas (Shull and Beckwith 1982; Gatley 1988), its distribution should delineate clearly the boundaries of the supersonic outflows, where they collide and shock the surrounding ambient cloud medium.

In this paper we present high-angular resolution pictures of the H_2 $v = 1$–0 $S(1)$ line emission from the shock-excited molecular jets associated with the luminous DR 21 and NGC 2071 star-forming molecular cloud complexes, and the less luminous, yet optically visible, HH 7–11 and HH 12 star-forming regions. These observations, which complement the low-angular resolution (5–20 arcsec) maps of integrated $S(1)$ emission and velocity-resolved $S(1)$ line profiles already obtained by us in previous investigations (Garden *et al.* 1986; Garden *et al.* 1989*a*; Burton, Geballe, and Brand 1989), *represent some of the highest angular resolution observations of molecular outflow sources yet obtained at any wavelength.* The observing technique is described in § II, the results are presented and discussed in § III, and the conclusions are given in § IV.

II. OBSERVATIONS

The H_2 $v = 1$–0 $S(1)$ emission-line images were obtained using an infrared camera (IRCAM) on the United Kingdom 3.8 m infrared telescope on the nights of 1987 November 8 and 9. IRCAM is a multipurpose instrument that is designed around a 62 × 58 array of InSb detectors (McLean 1987). A set of narrow-band (1%) filters were used to define the line emission and adjacent continuum. The observations were made in

[1] Alfred P. Sloan Fellow.

"stare mode" (i.e., no chopping of the secondary mirror) with a fixed image scale of 1.2 arcsec per pixel. The observing procedure consisted of the co-addition of two 200 s on-source integrations, followed by an integration of similar duration on a blank piece of sky offset a few arcmin from the source. The sky frames were used to flat field the source frames. Because many of the sources observed are significantly larger than the field of view of the array ($\sim 1'$ for the 1.2 arcsec per pixel scale), in most cases, it was necessary to mosaic several frames in order to obtain a complete picture of the source. An overlap interval between adjacent frames of approximately $\frac{1}{3}$ the array dimensions was used in order to adjust the DC (sky) levels of the individual frames to a common value and also to compensate for any small errors in the pointing between different positions. Owing to the relatively poor spectral resolution of the H_2 narrow-band filter, it was also necessary to obtain an estimate of the contamination due to continuum emission (i.e., from stars, hot dust, free-free emission, reflection nebulae, etc.). This was achieved by obtaining a single 60 s continuum image (1% filter at 2.104 μm) for every H_2 line image.

The method for data reduction is very similar to that used for reducing optical CCD images and basically consists of first substracting an instrumental bias (a very short exposure of a cold blocking aperture), ratioing the image frame by a normalized, median-filtered sky frame, and then subtracting a constant sky background flux to give a zero sky level. Approximate flux calibration was obtained by carrying out the same procedure on a standard star of known flux.

Unfortunately, as we found it difficult to accurately flux calibrate these images, their prime value is for their morphological, rather than flux, information. There are a number of reasons for this. To produce the final image, many frames had to be mosaicked together. When a frame contains extended, diffuse emission, as almost all of the frames do, it is difficult to distinguish between fluctuations in the sky background emission and intrinsic source emission. In addition, even if the frames where correctly mosaicked together and background fluxes correctly subtracted, since the 1% filter admits continuum radiation as well as line flux, any attempt to subtract the continuum from the line emission leads to large errors. Finally, misregistration, variable seeing over the course of the observations, and telescope motions during individual frames all conspire to make the subtraction of the continuum from the line (+ continuum) images highly undesirable as this results in a significant degradation in the quality of the original images. We therefore present only the line (+ continuum) images.

A scale bar is displayed below each image to act as both a rough calibration guide and to permit intercomparison between different images (the numbers on the scale bar are to be multiplied by 10^{-23} W cm^{-2} arcsec^{-2} to obtain flux units). As a check of the credibility of our flux calibration, we have integrated the H_2 $v = 1$–0 $S(1)$ line flux over the equivalent of a 20″ circular aperture positioned on the east and west peaks of the DR 21 jets. These positions were chosen because they are both bright in H_2 line emission and have negligible continuum emission. When compared with the more accurate single-beam flux measurements of Garden *et al.* (1986), we find that both data sets agree to within $\sim$20%. This is a good indication of the magnitude of the flux calibration errors inherent to the images presented in this paper.

III. RESULTS AND DISCUSSION

The results for each outflow source will now be presented and discussed in turn.

a) DR 21

i) *The Central Region*

Figure 1 (Plate 1) shows a continuum (1% filter at 2.104 μm) image of the central part of the DR 21 molecular cloud. This image shows that the near-infrared continuum consists of a bright central peak, surrounded by several weaker peaks; these may represent stars belonging to a compact stellar cluster or just density enhancements that are illuminated by a single central star. The brightest near-infrared continuum peak (DR 21 IRS 1) has the following 1950 coordinates; R.A. = $20^h37^m13^s.4$, Decl. = 42°08′59″. The DR 21 molecular cloud core, which lies to the east of this position, is totally opaque at near-infrared wavelengths (see Fig. 3). In particular, the luminous DR 21 compact H II region, which is a strong emitter at radio wavelengths (Harris 1973; Dickel *et al.* 1986; Roelfsema, Goss, and Geballe 1989), lies within or behind the dense cloud core and thus cannot be seen in the near-infrared continuum due to extensive foreground extinction. There is a second region of near-infrared to excessive foreground extinction. There is a second region of near-infrared continuum emission that lies on the east side of the cloud core, roughly 30″ to the east of DR 21 IRS 1. This component is also seen in the radio continuum (Roelfsema, Goss, and Geballe 1989) and is probably an extension of the compact H II region. Apart from the bright near-infrared point source (W75S IRS 2), which lies approximately 1′ to the north of the DR 21 IRS 1 (see Fig. 3 and Fig. 4 [Pl. 3]), no other regions of extended continuum emission were found outside the area covered by Figure 1.

ii) *The Extended Outflow Lobes*

Figure 2 (Plate 2), which is a mosaic of 20 individual frames, shows the distribution of H_2 $v = 1$–0 $S(1)$ line emission (+ continuum) over the entire DR 21 outflow source. Figure 3 presents a sketch of this image indicating the location of stars, extended continuum emission, and other features of interest. The field stars can easily be recognized since they appear as bright unresolved point sources. This image is in excellent agreement with the lower angular resolution observations presented previously by Garden *et al.* (1986, 1989*a* and 1989*b*), where it was suggested that DR 21 is probably the largest (extends over a projected distance of 5 pc), most massive ($M_{\rm outflow} > 1000\ M_\odot$), and most energetic ($E_{\rm outflow} > 3 \times 10^{48}$ ergs) young stellar outflow source yet known.

The increased angular resolution of the current observations bring to light several important new features that are worthy of mention.

i. The outflow lobes appear to narrow with increasing outward displacement from the outflow center (denoted by a diamond in Fig. 3) and eventually converge toward apices located several parsecs from the DR 21 cloud core. This may result from some kind of pressure-confinement mechanism, either magnetic or thermal. Considering our current lack of understanding of the distribution and strength of magnetic fields in different molecular cloud environments, we are reluctant to pursue the magnetic confinement model as we feel that such a discussion would be too speculative at this early stage. On the other hand, a calculation of the importance of thermal pressure confinement is relatively straightforward. Indeed, Garden *et al.* (1989*a*) show that, providing the high-velocity wind internal to the DR 21 jets is composed of a warm (several hundred K), presumably atomic, gas of relatively low density (several thousand cm^{-3}), then the collimation of the jets can result from the thermal pressure of the surrounding ambient molecular cloud. The proposed atomic wind, which may arise

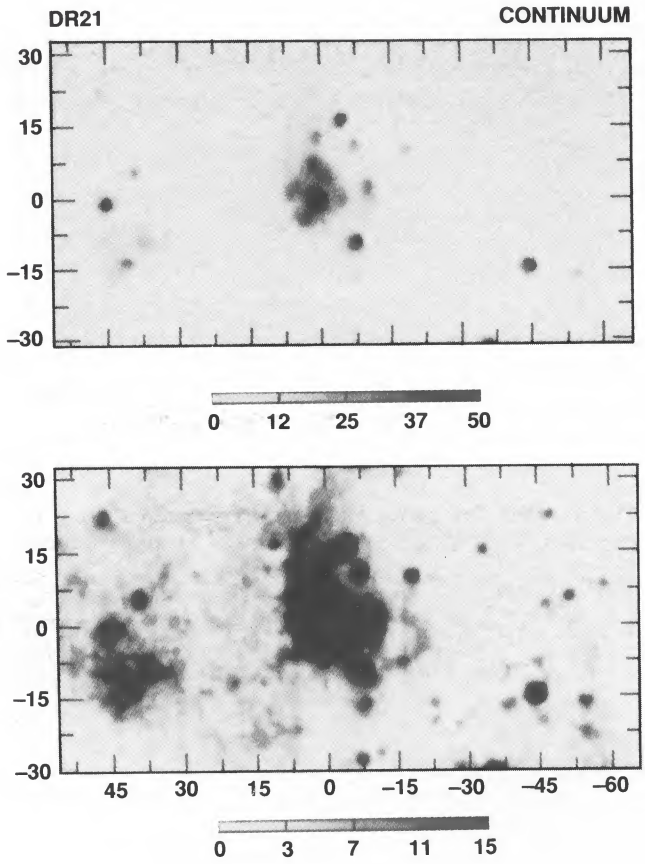

FIG. 1.—High and low contrast images of the DR 21 ultracompact H II region observed through a 1% resolution and continuum filter at 2.106 μm. The filter does not include emission from the H_2 $v = 1$–0 $S(1)$ line. The gray-scale bar at the bottom is in flux units of 10^{-23} W cm^{-2} arcsec^{-2}. The spatial offsets are in arcseconds and the (0, 0) position is centered on DR 21 (IRS 1) at R.A. = $20^h37^m13^s.4$, Decl. = 42°08′59″.

GARDEN *et al.* (*see* **354**, 233)

PLATE 2

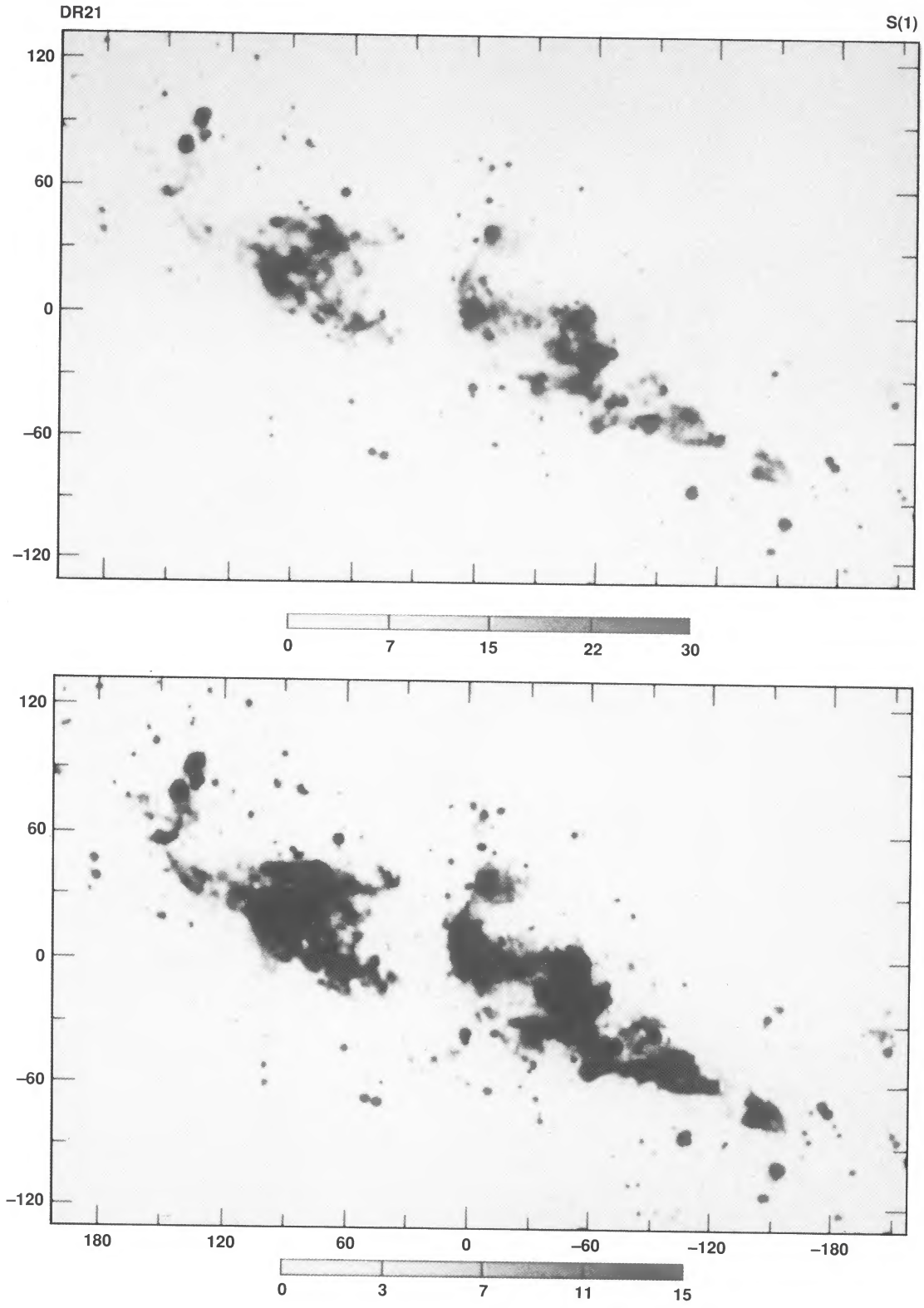

BURTON - 10

FIG. 2.—High and low contrast images of the H_2 $v = 1$–0 $S(1)$ line (+ continuum) at 2.122 μm in DR 21, observed through a 1% resolution filter centered on the $S(1)$ line with a plate scale of 1.2 arcsec per pixel. Fig. 3 provides further details, including the location of stars and continuum sources. The gray-scale bar at the bottom is in flux units of 10^{-23} W cm^{-2} arcsec^{-2}. The spatial offsets are in arcseconds and the (0, 0) position is centered on DR 21 (IRS 1) at R.A. = $20^h37^m13\overset{s}{.}4$, Decl. = 42°08′59″.

GARDEN *et al.* (*see* **354**, 233)

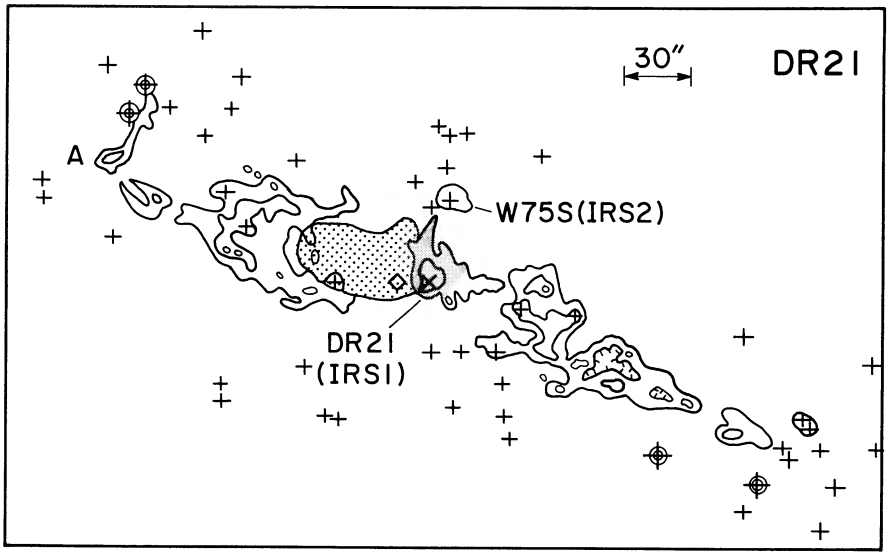

FIG. 3. Schematic outline of the molecular hydrogen (H_2) $v = 1$–0 $S(1)$ line emission from DR 21 (see Figs. 1, 2, and 4). The contour lines denote the extent of the $S(1)$ line emission, the dot-shaded area the region of 6 cm radio emission (Roelfsema, Goss, and Geballe 1989), and the line-shaded area a region of extended 2 μm continuum emission associated with the IR cluster at the core of DR 21. Crosses denote the location of stars seen in the image and the diamond the position of the CO outflow center (Garden *et al.* 1989). The "A" refers to the location of the sharp bend in the jet referred to in the text. The position of W75S (IRS 2) is labeled.

from either the recombination of an ionized circumstellar stellar wind or the dissociation of ambient molecular gas in high-velocity shocks, has recently been discovered in the 21 cm line of atomic hydrogen (A. Russell 1989, private communication). These new observations show that the atomic wind is highly collimated along an axis parallel to the major axis of the DR 21 H_2 jets, thus lending considerable support to the thermal confinement model.

ii. The H_2 line emission is extremely clumpy and shows considerable structure, all the way down to the smallest scales measurable with the array (2 arcsec $\equiv$ 0.02 pc for $d = 2.5$ kpc). This suggests either that the ambient cloud is itself clumpy, or that an additional mechanism associated with the jets, such as the generation of oblique internal shocks or shear instabilities along the jet walls, produces these clumps. It is inevitable that some of the clumpy structure, especially toward the innermost parts of the jets, results from the obscuration of the near-infrared radiation by dense foreground material. This, however, is probably not true for the bulk of the jet emission which lies sufficiently far from the dense molecular cloud core to be relatively unaffected by foreground extinction (see § III*a*iii). In any case, the complex internal structure of the DR 21 jets suggests the presence of highly turbulent internal motions that may help explain the significant variations in the shape and width of the H_2 $S(1)$ line profiles previously observed by Garden *et al.* (1989*a*).

iii. The eastern lobe exhibits a peculiar phenomenon at its outer extremity, where the direction of propagation of the jet changes suddenly through a projected angle of 90° (see component A of Fig. 3). In (i) we noted that our observations suggest that the H_2 jets become more collimated with increasing distance from the DR 21 cloud core. As discussed in (ii), this may result from a pressure imbalance between the jet material and the surrounding molecular cloud. It therefore seems plausible that the eastern H_2 jet is indeed quite narrow at its end and that the sudden change in direction results from interaction with some external agency, such as the collision of the jet with a massive clump in the ambient molecular cloud.

The various physical processes that shape the DR 21 H_2 jets are probably also common to the other outflow sources discussed in this paper. A more detailed discussion of these processes, with particular reference to the HH 7–11 outflow, can be found in § III*c*iii.

iii) *Extinction*

As discussed by Righini-Cohen, Simon, and Young (1979), Harvey *et al.* (1986), and Garden *et al.* (1989*b*) the foreground optical extinction toward the central core of the DR 21 molecular cloud exceeds 100 mag but decreases rapidly with outward displacement from the central cloud core, falling to $10 > A_v(\text{mag}) > 30$, at the innermost peaks of the H_2 emission-line jets (Garden *et al.* 1986). Although the near-infrared extinction associated with the extended H_2 outflow lobes is significant [$1 > A_{2.1\,\mu\text{m}}(\text{mag}) > 3$] and undoubtedly blocks much of the diffuse H_2 line emission, it is not of sufficient magnitude to seriously affect the intrinsic morphology of the brightest emission-line peaks. In particular, we argue that the overall bipolar shape and increasing degree of collimation of the H_2 jets are intrinsic features of the source and are *not the result of obscuration by clumpy foreground material.* This, we believe, is also true of the jetlike structures seen toward the other embedded sources discussed in this paper (i.e., NGC 2071 and HH 7–11). Additional evidence in support of this claim derives from the morphological similarity exhibited between the near-infrared H_2 and high-velocity CO (Garden *et al.* 1989*b*) and HCO^+ (Grolemund, Garden, and Carlstrom 1989, in preparation) line emission, which would not result if the H_2 emission were seriously affected by heavy foreground extinction. This particular argument also applies in the case of NGC 2071 and HH 7–11, to be discussed later in this section.

iv) *The Origin of the Ionized Gas in the Eastern Lobe*

Harris (1973) and Roelfsema, Goss, and Geballe (1989) have observed the compact DR 21 H II region at centimeter wave-

lengths using radio interferometers. Harris found that the radio continuum emission is sharply peaked at the position of DR 21(S) and displays a significantly weaker extension to the east. The more recent observations of 6 cm radio continuum emission made by Roelfsema *et al.* have significantly higher spatial resolution and consequently show the eastern extension to the compact DR 21 H II region much more clearly. At the outer extremity of the eastern extension the radio continuum brightens to form a narrow ridge of enhanced emission that presumably delineates the H II region/molecular cloud boundary.

In order to investigate the spatial relationship between the ionized and shock-excited molecular gas at the inner edge of the eastern H_2 lobe (there is no ionized gas associated with the western lobe; Garden *et al.* 1986), a Brγ (2.166 μm) line (+ continuum) image was obtained. This image, which was taken through a 1% narrow-band filter, is compared with the H_2 $S(1)$ line (+ continuum) image in Figures 4 and 5 (Plates 3 and 4). The central DR 21 near-infrared source (labeled DR 21 IRS 1 in § III*ai*) is composed mainly of continuum emission (see Fig. 1) that probably arises from hot dust heated by the ionizing photons of the central O star cluster (Harris 1973; Roelfsema, Goss, and Geballe 1989). The bright near-infrared point source, W75S IRS 2, located at the top of both images, is also a strong continuum source. There is, however, a significant difference in the appearance of the two images on the eastern side of the molecular cloud; the regions of H_2 $S(1)$ and Brγ line emission are clearly separated, with the Brγ appearing to form a shell (similar to that observed in the radio continuum) that is located along the inside boundary of the eastern H_2 outflow lobe.

There are several possible models that may explain the observed spatial displacement of the H_2 and Brγ line emission in the eastern lobe. We discuss three of them here.

i. The Brγ line emission may come from an *expanding ionization front*, which is fueled by energetic photons emanating from the central O star (cluster). The pressure within the ionized gas drives a shock into the molecular cloud, exciting vibration H_2 line emission. A serious drawback to this model, however, is that it is hard for an expanding H II region to drive a shock sufficiently fast into molecular gas to excite significant quantities of vibrational H_2 line emission (Hill & Hollenbach 1978; Garden *et al.* 1986).

ii. The ionized gas may result from the *dissociation and ionization of molecules in a fast shock* (i.e., $V_{\rm shock} > 50$ km s^{-1}). In this scenario, a high-velocity atomic wind (as observed in 21 cm H I line emission by A. Russell [1989, private communication]) collides with the ambient cloud medium, initiating the propagation of a slow shock into the dense molecular cloud, and an oppositely directed fast ionizing shock into the wind. The two shock fronts (slow/molecular and fast/ionized) are thus spatially separated on the sky with the ionized gas lying internal to the shocked molecular shell.

For a fast, jump shock where collisional ionization is balancing radiative recombination and where the shock totally ionizes the gas (Burton *et al.* 1989), the flux from Brγ, per square arcsec on the sky, not corrected for extinction is

$$\mathscr{F}(\mathrm{Br}\gamma) = 1.0 \times 10^{-21}(n_0/10^5\ \mathrm{cm}^{-3})(V_s/100\ \mathrm{km\ s}^{-1}) \mathrm{W\ cm}^{-2}\,\mathrm{arcsec}^{-2}, \quad (1)$$

where n_0 is the preshock molecular cloud density and V_s is the shock velocity. Thus, for a range of 2.12 μm extinction, $1 < A_{2.1\,\mu\mathrm{m}}(\mathrm{mag}) < 3$ (Garden *et al.* 1986), we predict the following range of Brγ line flux: $7 \times 10^{-23}(n_0/10^5\ \mathrm{cm}^{-3})(V_s/100\ \mathrm{km\ s}^{-1}) < \mathscr{F}(\mathrm{Br}\gamma)(\mathrm{W\ cm}^{-2}\ \mathrm{arcsec}^{-2}) < 4 \times 10^{-22}\ (n_0/10^5\ \mathrm{cm}^{-3})(V_s/100\ \mathrm{km\ s}^{-1})$. In comparison, the peak Brγ line flux measured in Figures 4 and 5 is $\sim 5 \times 10^{-22}$ W cm^{-2} arcsec^{-1}. It therefore appears that a shock traveling at high velocity ($V_s > 100$ km s^{-1}) into a dense ($10^5 < n_0(\mathrm{cm}^{-3}) < 10^6$) molecular cloud may be able to produce both the morphology and range of intensities observed in Brγ emission. Velocity-resolved observations of the Brγ line are required in order to test this hypothesis as the line profile should display broad wings.

iii. It is possible that some of the H_2 line emission may arise from a *dense photodissociation region* (PDR; e.g., Tielens and Hollenbach 1985), with the Brγ emission originating from the inside edge of the PDR, facing the source of UV photons. This suggestion is supported by the observation of fine-structure lines of [O I], [Si II], and [C II] (Lane *et al.* 1989) in the far-infrared. Lane *et al.* argue that the relative strengths of these lines requires a PDR model rather than shocked emission. We find, however, from a comparison of the available UV and observed H_2 line fluxes (Garden *et al.* 1986), that it is possible to account for no more than 10% of the observed H_2 $S(1)$ line emission by photoelectric heating of the gas alone. Therefore, although a PDR is almost certainly present, a significant portion of the H_2 line emission in the eastern lobe is still shock excited.

To summarize, we find that model (ii), the dissociation and ionization of molecules in a fast shock, best fits the Brγ and H_2 line observations of the eastern lobe. However, it is most likely that the overall picture is not this simple and that the solution probably involves some complex mixture of a high-velocity shock and a PDR, the relative importance of which remains to be determined from further observations. For example, measurements of the velocity profiles of the H_2, Brα, and far-infrared, fine-structure lines would facilitate a definitive test, since PDRs and shocks are characterized by narrow and broad lines, respectively.

b) NGC 2071

i) *The Central Region*

Figure 6 (Plate 5) shows a comparison of the 2.104 μm continuum and 2.122 μm H_2 $v = 1$–0 $S(1)$ line (+ continuum) emission in the central part of the NGC 2071 young stellar outflow. The continuum image reveals clearly the presence of several bright near-infrared point sources that are presumably young stars that have recently formed from the molecular cloud. Previous observations at 10 μm (Persson *et al.* 1981) have already identified the existence of three infrared sources: IRS 1, 2, and 3 (see Fig. 8). The two brightest infrared sources, IRS 1 and IRS 2, are joined by a bridge of weaker emission while IRS 3, which is located about 5″ north of IRS 1, is considerably fainter than either IRS 1 or IRS 2. The two bright point sources located just north of the IRS 1/2/3 young stellar cluster are foreground stars and as such are of no importance to the discussion. The emission in the H_2 line (+ continuum) image is more extended and shows considerably more structure than that in the continuum image. The most prominent feature is a narrow jet of H_2 line emission which appears to originate from the west side of the young stellar cluster, close to IRS 1, and curves northward. The jet is composed of several bright clumps that are interconnected by weaker H_2 line emission. There is no evidence for a similar jetlike feature protruding to the south of the stellar cluster.

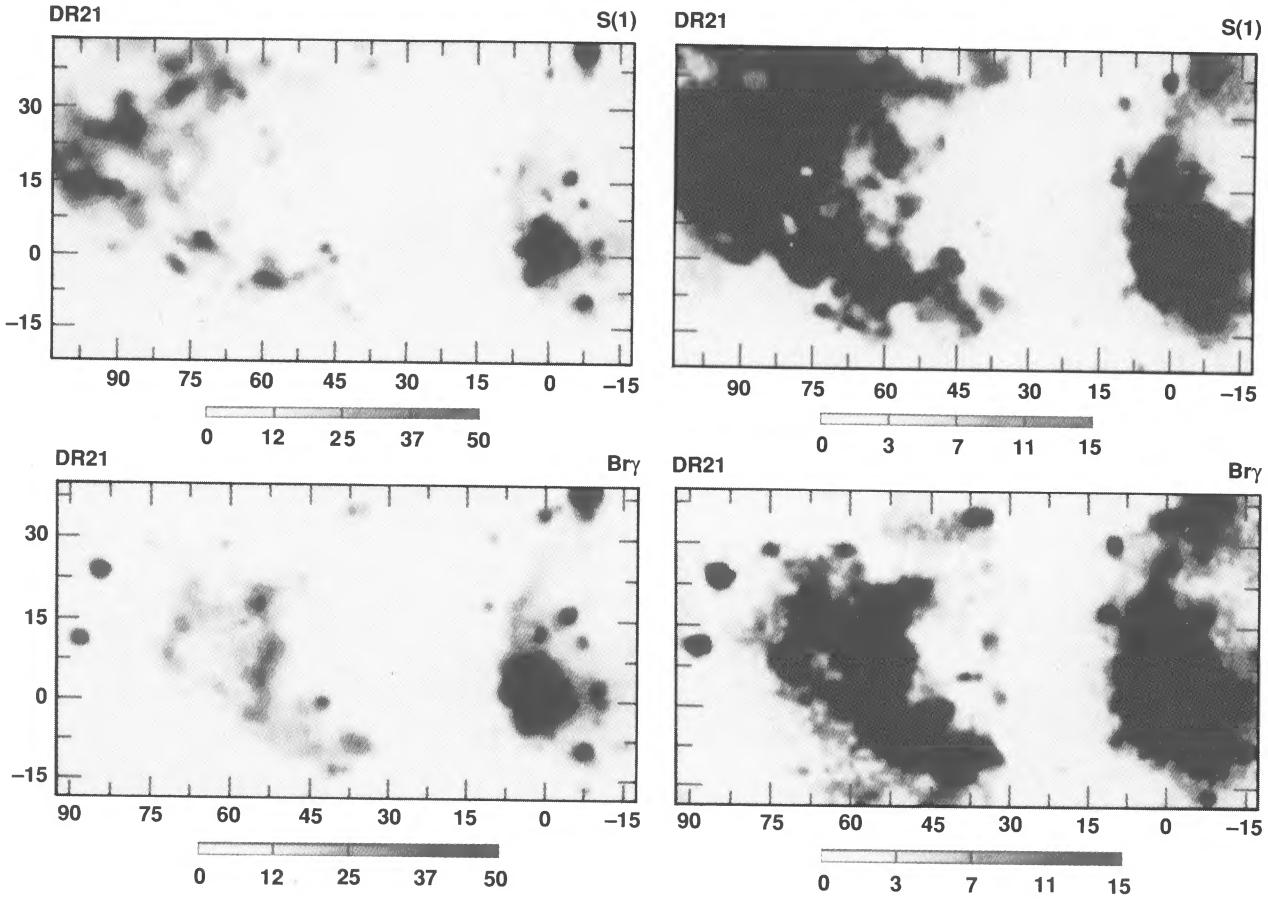

BURTON - 2

FIG. 4.—High and low contrast images of the H_2 $v = 1$–0 $S(1)$ line (*top*) and the 2.166 μm hydrogen Brγ line (*bottom*) in the core of DR 21, observed through the 1% resolution filters centered on the lines. Regions of continuum emission can be ascertained by inspection of Fig. 1. The gray-scale bar at the bottom of each image is in flux units of 10^{-23} W cm^{-2} arcsec^{-2}. The spatial offsets are in arcseconds, and the (0, 0) position is centered on DR 21 (IRS 1) at R.A. = $20^h37^m13^s.4$, Decl. = 42°08′59″.

GARDEN *et al.* (*see* **354**, 235)

PLATE 4

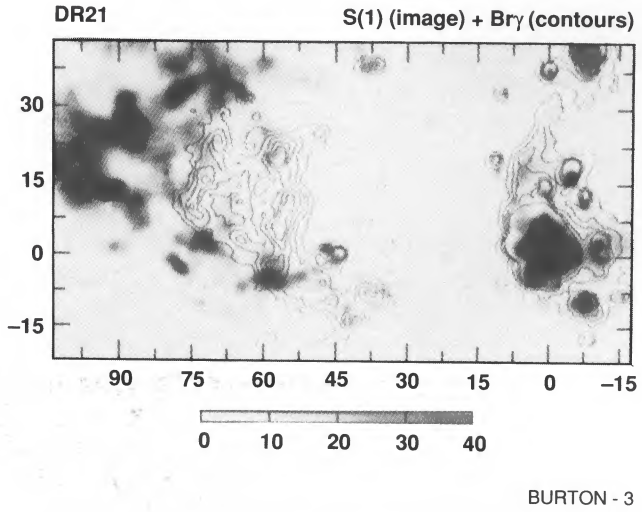

FIG. 5.—Same as for Fig. 4, but this time the Brγ emission (*contours*) is superposed directly on the H_2 $v = 1$–0 $S(1)$ line image (*gray scale*).

GARDEN *et al.* (*see* **354**, 235)

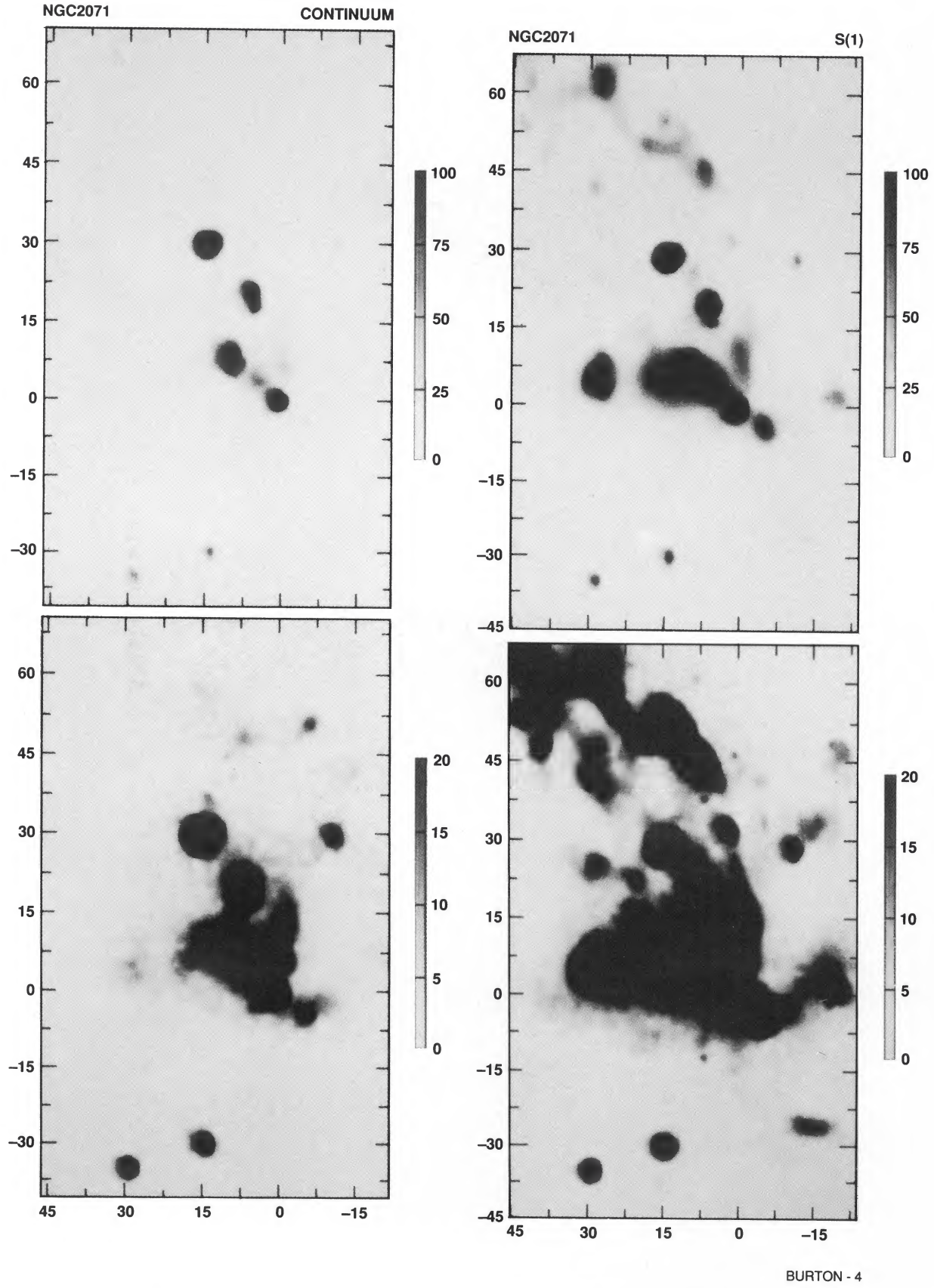

FIG. 6.—Images of the outflow center on NGC 2071. *Left:* high and low contrast images at the continuum at 2.106 μm. *Right:* high and low contrast images of the H_2 $v = 1$–0 $S(1)$ line (+ continuum), through the 1% filter. The gray-scale bar at the bottom of each image is in flux units of 10^{-23} W cm^{-2} arcsec^{-2}. The spatial offsets are in arcseconds, and the (0, 0) position is centered on NGC 2071 (IRS 1) at R.A. = $5^h44^m30^s.6$, Decl. = 00°20′41″ (Bally and Predmore 1983).

ii) *The Extended Outflow Lobes*

The distribution of H_2 $v = 1$–0 $S(1)$ line (+ continuum) emission over the entire NGC 2071 young stellar outflow is shown in Figure 7 (Plate 6), which is a mosaic of 20 frames. Figure 8 presents a sketch of this image indicating the location of stars, extended continuum, and other features of interest. Apart from stars, no additional continuum emission was found outside of that displayed in Figure 6. Our H_2 emission-line image, which is in excellent agreement with the lower angular resolution (20″) H_2 $S(1)$ line maps presented previously by Lane and Bally (1986) and Burton, Geballe, and Brand (1989), shows that the H_2 line emission is bipolar with an axis and spatial extent similar to that of the CO outflow (Snell *et al.* (1984). This close association suggests that the H_2 is shock-excited by the same high-velocity winds that drive the molecular outflows.

The increased angular resolution of the current observations bring to light several important features that are worthy of mention.

i. In the blueshifted CO flow (northeastern lobe) the H_2 line emission appears to form a well-collimated jet that is composed of several regularly spaced knots that are joined by fainter emission. Halfway along its length the jet suddenly breaks, undergoes a dramatic change of direction, and then continues parallel to its original course. We can only speculate that this results from the collision of the jet with a massive clump in the ambient cloud medium (cf. the tip of the eastern H_2 jet in DR 21).

ii. There is a clear absence of H_2 emission immediately south of the central infrared cluster. Lane and Bally (1986) initially ascribed to this gap to extinction by a flattened structure at right angles to the flow; presumably a disk of some sort. However, in a subsequent paper (Bally 1986), it was shown that the high-velocity 21 cm H I line emission from NGC 2071 also exhibits the same gap. This led Bally to conclude that "the gap seen in the 2.12 μm observations is probably real and not an artifact caused by foreground extinction." This point is discussed further by Burton, Geballe, and Brand (1989). What then is the origin of the gap? We suggest three plausible scenarios, namely (i) the H_2 molecules are dissociated in shocks with a high-velocity wind, (ii) the cloud density is too low at this position ($< 10^3$ cm^{-3}) to excite vibrational H_2 line emission, or (iii) the wind is freely expanding into a preexisting cavity. Due to the fact that the H_2 and H I peaks are anti-correlated (the H I peaks closer to the outflow center than does the H_2), both Bally (1986) and Burton, Geballe, and Brand (1989) favor the first scenario in which the H_2 is dissociated in high-velocity shocks, thus producing an abundance of atomic

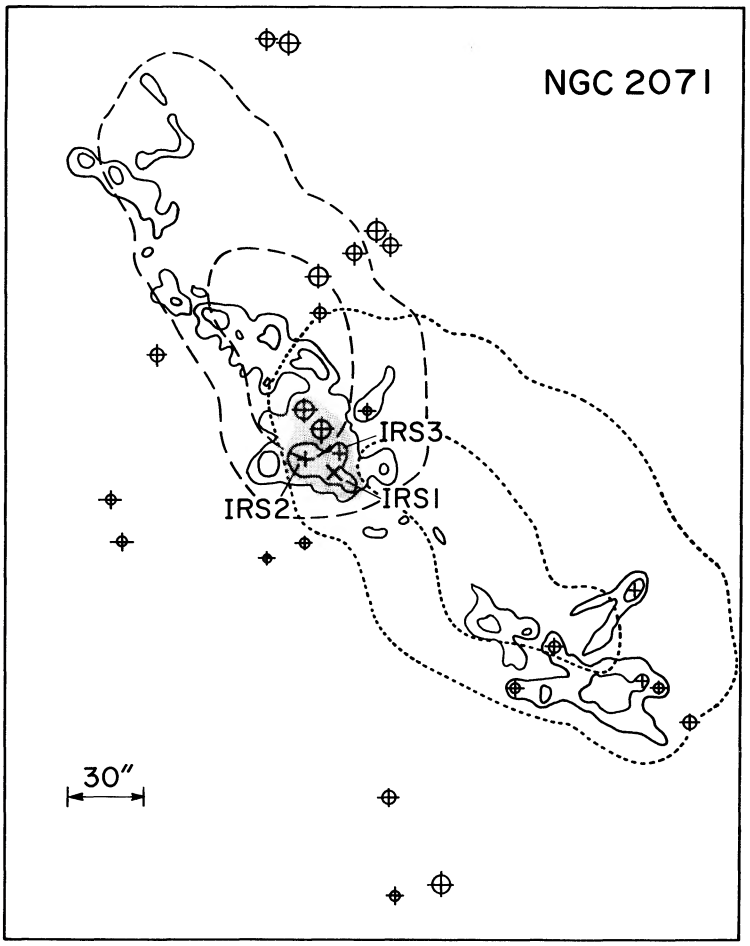

FIG. 8.—As for Fig. 3, a schematic diagram of the H_2 $v = 1$–0 $S(1)$ line emission from a NGC 2071 (see Figs. 6 and 7). The locations of the infrared sources IRS 1, IRS 2, and IRS 3, a region of extended 2 μm continuum emission (*line-shaded region*) and field stars (*crosses*) are shown. The dashed contours show the blueshifted CO $J = 2$–1 outflow lobe and the dotted contours the redshifted lobe (Snell *et al.* 1984).

PLATE 6

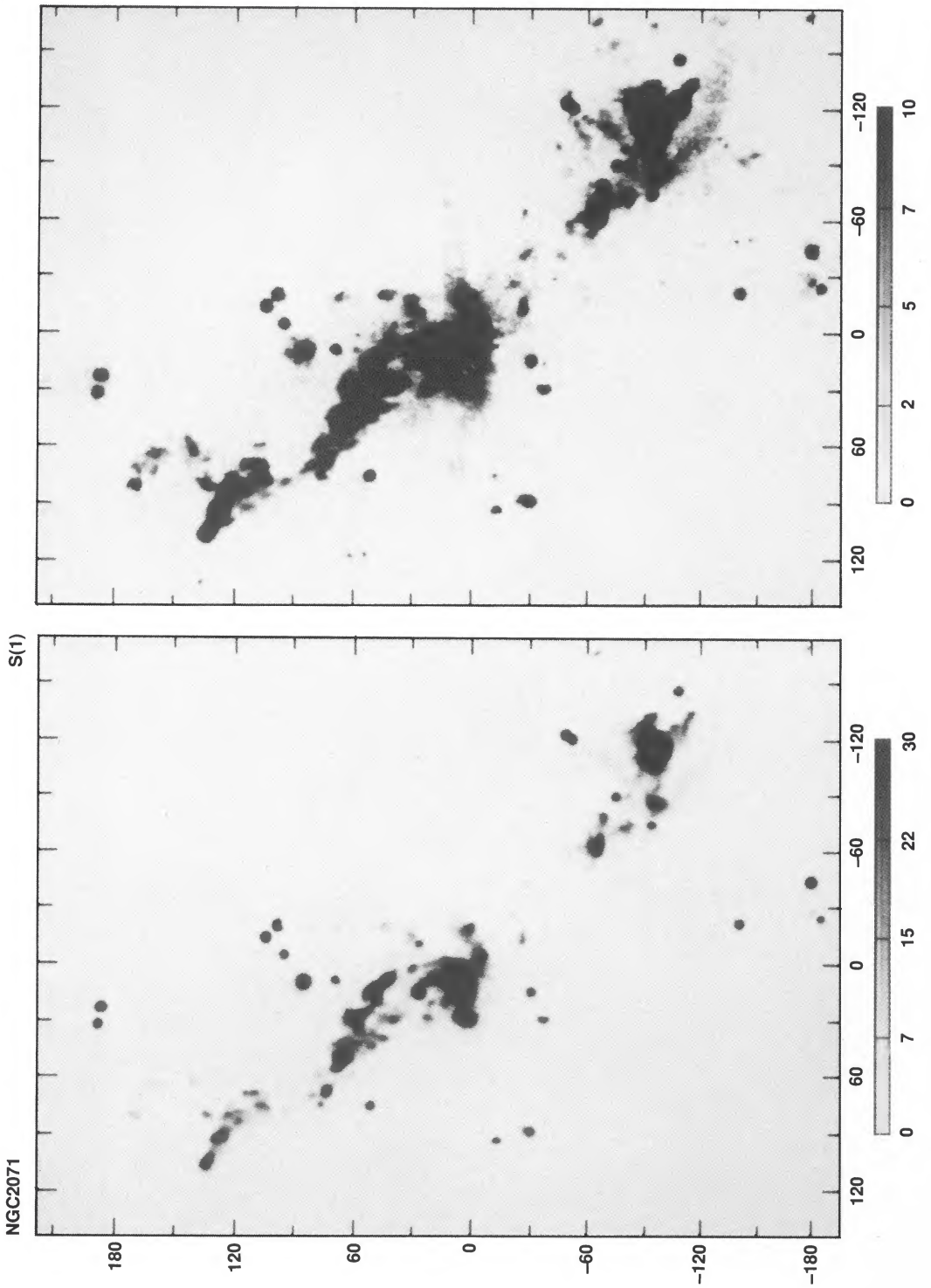

FIG. 7.—High and low contrast images of the H_2 $v = 1$–0 $S(1)$ line (+ continuum) in NGC 2071, observed through a 1% resolution filter, with a plate scale of 1.2 arcsec per pixel. Figure 8 provides further explanatory information. The gray scale at the bottom of each image is in flux units of 10^{-23} W cm^{-2} arcsec^{-2}. The spatial offsets are in arcseconds, and the (0, 0) position is centered on NGC 2071 (IRS 1) at R.A. = $5^h44^m30^s.6$, Decl. = 00°20′41″ (Bally and Predmore 1983).

GARDEN *et al.* (*see* **354**, 236)

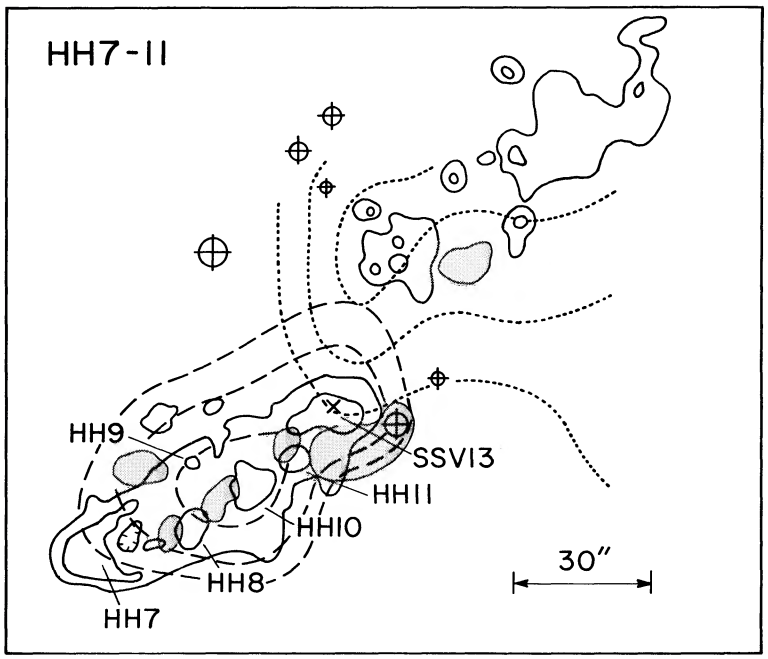

FIG. 10.—As for Fig. 3, a schematic diagram of the H_2 $v = 1$–0 $S(1)$ line emission from HH 7–11 (see Fig. 8). In addition, the positions of the Hα knot HH 11 and of SSV 13, the presumed driving source of the outflow, are shown. The shaded areas denote the locations of the HCO^+ knots observed by Rudolph and Welch (1988). The molecular outflow, as mapped in the $J = 2$–1 CO line with an angular resolution of 20″, is also shown; dashed contours show the blueshifted CO emission and the dotted contours the redshifted emission.

hydrogen close to the outflow center where the wind velocity is presumably highest. The H_2 emission does not turn on until further out in the flow, when the wind velocity has decelerated to below the dissociation velocity (~ 50 km s^{-1}, at which time the production of atomic hydrogen ceases and the H I emission dies off.

iii. Toward the end of the redshifted CO flow (southwestern lobe), the H_2 line emission reappears in the form of several distinct knots; the brightest of these lies at the extreme outer edge of the CO outflow. It is exciting to postulate that this H_2 emission-line clump may represent the "working surface," where the high-velocity flow collides with the ambient cloud medium.

iv. The size of the H_2 emission-line clumps in both the blue and redshifted jets are comparable to those observed in DR 21, being of order 0.01–0.05 pc. If these shocked molecular clumps have internal densities, $n > 10^5$ cm^{-3} (necessary in order to excite vibrational H_2 line emission), then the above range in clump size corresponds to a range in mass of 2×10^{-2} to 3 $M_\odot$. The clumps may form either as a result of hydrodynamic instabilities in a pressure-confined jet flowing along a strong density gradient (e.g., Königl 1982; Norman, Smarr, and Winkler 1986; Canto, Tenorio-Tagle, and Rozyczka 1988) or, from the growth of nonlinear Kelvin-Helmholtz instabilities along the walls of the jet (see, e.g., Payne and Cohn 1985; Buhrke, Mundt, and Ray 1988). Alternatively, the knots may represent preexisting clumps of ambient gas that have been swept up and illuminated by interaction with a high-velocity atomic wind (Bally 1986). A more detailed discussion of these clump-forming processes is given in § III*c*iii).

c) HH 7–11

i) *The Bipolar Jets*

HH 7–11 has been extensively studied at both high-spectral and spatial resolution in the optical (Solf and Bohm 1987) and is a previously known source of vibrational H_2 line emission (Zealey, Williams, and Sandell 1984; Lightfoot and Glencross 1986). Our image of H_2 $v = 1$–0 $S(1)$ line (+ continuum) emission is shown in Figure 9 (Plate 7) and a sketch of the image is shown in Figure 10. The source of the high-velocity winds is believed to be low-mass star SSV 13 (Grossman *et al.* 1987). The redshifted molecular flow propagates to the northwest, and the blueshifted flow to the southeast, of SSV 13. The (0, 0) position in Figure 9 is taken to coincide with the location of SSV 13. Just to the west of SSV 13 there lies a bright field star (no. 6 in the notation of Herbig and Jones 1983) that lies on the same frame as SSV 13. Using the position for star no. 6 as given by Herbig and Jones and applying our measured offsets from this star to SSV 13, we calculate that the position of SSV 13 is R.A. = $3^h25^m58^s.1$ ($\pm 0^s.1$), Decl. = 31°05′45″.0 ($\pm 1''.0$).

We list below several interesting features of the HH 7–11 H_2 S(1) line (+ continuum image that are worthy of mention.

i. Although the outflow is known to be bipolar from millimeter-wave studies, only the southeaster (blueshifted) jet is visible at optical wavelengths. However, Figure 9 shows clearly that the northwestern (redshifted) jet is indeed present and is easily distinguishable in infrared H_2 line emission. This result is not entirely unexpected as the redshifted jet, which is moving into the molecular cloud, experiences significantly more extinction than the blueshifted jet.

ii. In the southeastern (blueshifted) jet, the Herbig-Haro objects form a series of bright, shock-excited knots that are regularly placed along the entire length of the jet. The outermost knot (HH 7) shows a beautiful example of a bow shock where the high-velocity jet collides with the ambient cloud medium to form a curved shock front that bends backward along both sides of the jet. The other knots (HH 8, 9, 10, and 11) appear to be immersed in a more diffuse halo of shocked gas that fills the remainder of the jet. The diffuse component

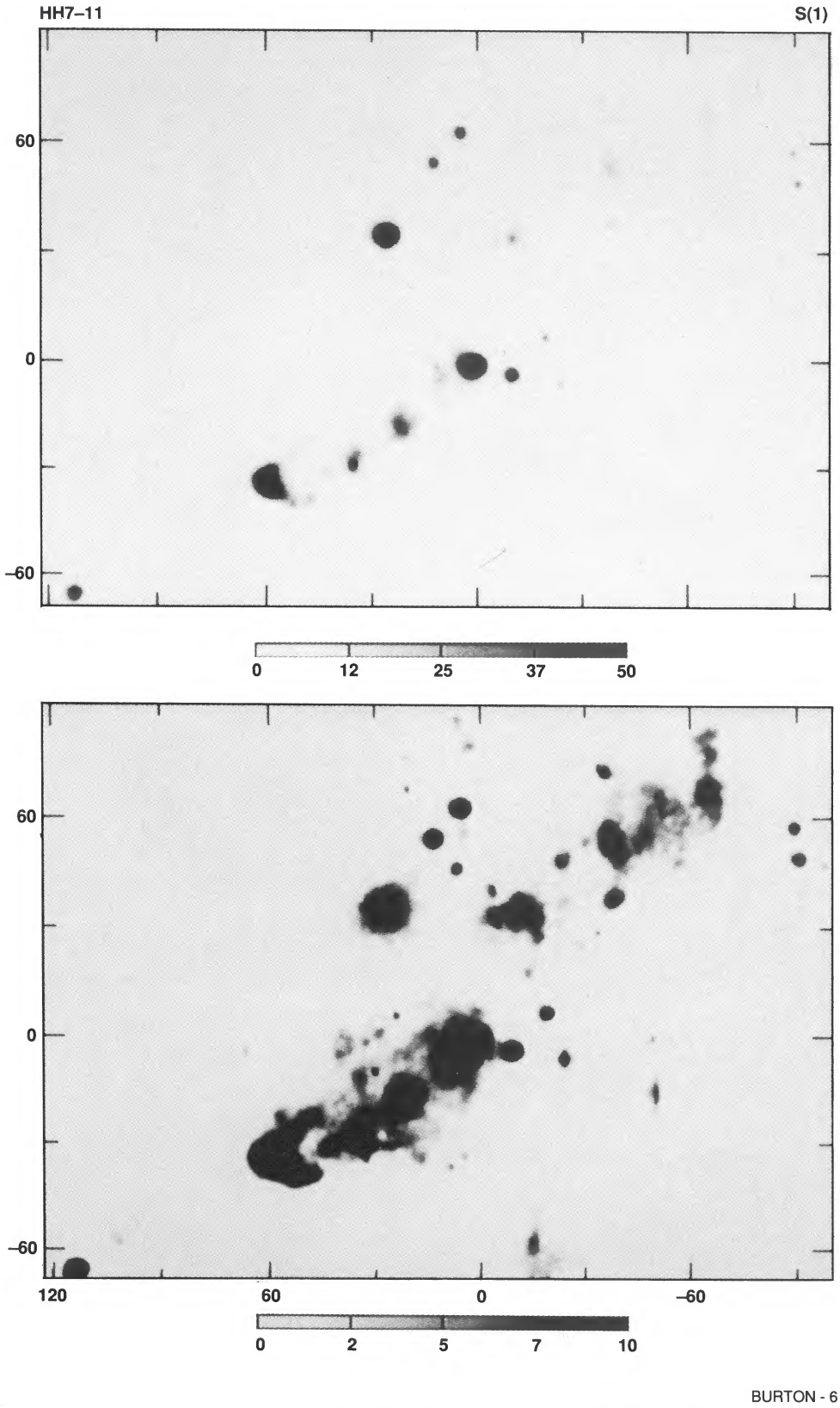

FIG. 9.—High and low contrast images of H_2 $v = 1$–0 $S(1)$ line (+ continuum) emission in HH 7–11, observed through a 1% resolution filter, with a plate scale of 1.2 arcsec per pixel. Fig. 10 provides further explanatory information. The gray-scale bar at the bottom of each image is in flux units of 10^{-23} W cm^{-2} arcsec^{-2}. The spatial offsets are in arcseconds, and the (0, 0) position is centered on SSV 13 at R.A. = $3^h25^m58^s.1$, Decl. = 31°05′45″ (this paper).

may result from the backflow of shocked gas that is generated at the jet terminus and swept backward by the ram pressure of the ambient cloud medium (Rozyczka and Tenorio-Tagle 1985). It is also worth noting that both HH 9 and HH 11 appear to be considerably fainter in H_2 line emission than HH 7, 8, and 10.

iii. In contrast to the spectacular morphology found in the southeastern jet, the northwestern (redshifted) jet is significantly weaker, exhibits little internal structure, and lacks a bright bow shock at its end. Instead it appears to narrow at its end and quietly disappears into the surrounding medium.

iv. Although both jets of H_2 line emission are oriented parallel to one another, there appears to be a significant spatial offset between the axes of the two; the axis of the northwestern jet being offset 25″ to the NE from the axis of the southeastern jet. As is discussed in the next section, this behavior is also seen for the blue and redshifted lobes of ^{12}CO $J = 2$–1 line emission and therefore is unlikely to be due to foreground extinction in the red lobe.

ii) *Comparison with Optical and Millimeter Line Emission*

A comparison of the H_2 $S(1)$ line image with optical images of the Hα line (Mundt 1984) shows that both the shock-excited ionized and molecular gas components (HH 7, 8, 9, 10, and 11) are spatially coincident to within our pointing errors (<2″) and are of comparable shape and size. It is unlikely that the H_2 $S(1)$ and the Hα lines originate from the same volumes of space due to the very different conditions required for their excitation. The observed spatial coincidence of the H_2 and the Hα line emission therefore suggests that the emission may originate from numerous small clumps of ionized and molecular gas that have scale sizes much smaller than the available spatial resolution of the infrared array (i.e., 0.005 pc at a distance of 500 pc). Providing the clumps are sufficiently mixed, then, when averaged over the spatial resolution of the infrared observations, the result appears as nearly identical morphologies for the H_2 and Hα lines.

An alternative explanation for the coincidence of the Hα and H_2 $S(1)$ line emission is that the Hα is produced in fast, dissociative shocks ($V_s > 50$ km s^{-1}), with the H_2 line emission arising from reformed molecules downstream of the shock (see, e.g., Hollenbach & McKee 1989). In this scenario, the spatial separation between the Hα and H_2 line-emitting regions is less than 1″ at the distance of NGC 1333. For HH 7, for which detailed line spectra are available (Burton *et al.* 1989), the measured H_2 $v = 1$–0 $S(1)$ line flux, 4×10^{-4} ergs cm^{-2} s^{-1} sr^{-1}, is consistent with the upper end of the flux range predicted by the dissociative shock models. However, the models predict a line ratio for the 1–0 $S(1)$/2–1 $S(1)$ lines of 2–3, whereas the observed value in HH 7 is 10, a value typical of emission from shocked rather than reformed molecular hydrogen. Nonetheless, the details as to the formation spectrum are uncertain, and this model may merit closer attention if the process becomes better understood.

Figure 10 also shows an outline of a 20″ resolution map of ^{12}CO $J = 2$–1 emission made with the James Clerk Maxwell telescope (W. Dent & A. Russell, private communication). It is interesting to note that the blue and redshifted CO outflow lobes have the same spatial offset as the H_2 jets. One possible explanation for this offset is that the initial outflow from SSV 13 is not directed along the large-scale axis of the outflow, but at an angle to it. Then as the flow develops, the ambient molecular cloud redirects the outflow along the direction of least resistance, thereby causing the observed spatial offset between the two lobes. This model has two important implications; first, the outflow must be pressure-confined away from the source (in order for the ambient cloud to be important dynamically), and second, the outflow must be collimated close to SSV 13.

Particularly intriguing is a comparison of our H_2 emission-line image with the millimeter interferometer map of HCO^+ line emission made by Rudolph and Welch (1988). As is shown in Figure 10, the knots of HCO^+ emission are observed displaced downwind (i.e., away from the driving source SSV 13) of the knots HH 8, HH 9, and HH 10. The HCO^+ knots are essentially at rest with respect to the ambient cloud and have narrow linewidths ($\Delta V < 0.5$ km s^{-1}), indicating that they are internally quiescent. In contrast, the Hα and H_2 emission-line knots are blueshifted 40 to 160 km s^{-1} with respect to the ambient cloud (Solf and Bohm 1987; Zinnecker *et al.* 1989). Rudolph and Welch propose that the slow-moving HCO^+ clumps that they observe are the material that shocks the stellar wind, thus forming the H-H objects. The lack of any HCO^+ emission associated with the HH 7 knot probably implies that this knot is freely moving into a much lower density medium than the material associated with the other knots. The bow-shock morphology and large blueshifted velocities of the shocked ionized and molecular emission associated with HH 7 suggests that either it is a clump of gas (i.e., a bullet) plowing into lower density ambient cloud material, or that it represents the "working surface" of the jet. It is worth noting that HCO^+ emission also arises from the prominent gap between the two regions of H_2 line emission in the redshifted (northwestern) jet (see Fig. 10). The HCO^+ emission here probably has a similar origin as that discussed for the blueshifted jet.

iii) *Models for the Jet Structure*

Any model of the HH 7–11 jets must explain the following kinematic and morphological relationships: (i) extremely high velocity 21 cm H I line emission (Lizano *et al.* 1988), (ii) high-velocity, blueshifted Hα line emission (Solf and Bohm 1987) that is associated with the optical Herbig-Haro objects, (iii) low-velocity, slightly blueshifted H_2 line emission that is spatially coincident with the ionized Herbig-Haro knots (Zinnecker *et al.* 1989; this paper), and (iv) dense clumps of quiescent molecular gas that lie between the Herbig-Haro knots (Rudolph and Welch 1988). We now suggest three models that may explain the above observation.

i. *The shocked cloudlet model.*—This model, which was also proposed by Rudolph and Welch (1988), assumes that the HCO^+ emission is formed on the upwind edges of dense, stationary, quiescent clumps that are being compressed by the atomic wind to a density above the critical density required for the excitation of HCO^+ $J = 1$–0 emission ($\sim 10^5$ cm^{-3}). The Hα and H_2 emitting regions then arise from the high-velocity wind and low-velocity clump shocks, respectively. The situation envisaged here is drawn schematically in Figure 11*a*. In this model, the collision of a collimated atomic wind (Lizano *et al.* 1988) with dense molecular clumps in the ambient cloud creates thin shells of shock-excited gas that envelope the clumps; the H_2 shells being located internal to the Hα. When viewed in projection, these shells appear spatially coincident. A potential problem with this model however is that the regular spacing of the Hα and H_2 emission-line knots along the southeaster (blueshifted) jet necessitates a correspondingly regular

density distribution in the ambient molecular cloud, which is highly unlikely considering the fact that molecular clouds are turbulent. This argument also applies in the case of the northeastern jet of the NGC 2071 young stellar outflow (see Fig. 7).

ii. *The pressure-confined jet model.*—Recently Canto, Tenorio-Tagle, and Rozyczka (1988) have shown that the focusing effect of a pressure-confined stellar wind leads to the formation of a narrow cylindrical stream or "jet" of reshocked stellar wind matter moving directly away from the central driving source at a high velocity. Furthermore, as the jet is injected into the surrounding cloud, it eventually reaches a point where it becomes overpressured relative to the surrounding ambient medium, it then expands until it becomes underpressured, at which point it converges, shocks itself, becomes overpressured, then reexpands, and so on (Königl 1982; Norman, Smarr, and Winkler 1984). Several cycles of contraction and reexpansion may occur thus producing a series of incident-reflected shock planes (or Mach disks) that are regularly spaced along the jet axis, with a separation of order a few times the jet width. The situation envisaged here is illustrated schematically in Figure 11*b*. The Hα and H_2 emission-line knots are formed at the compression nodes of the jet where the oblique, internal shocks meet. On the other hand, HCO^+ knots are formed along the expanding parts of the jet where slow external shocks are injected into the surrounding molecular cloud medium, thus forcing the gas density above the critical density for excitation of HCO^+. As the Hα and H_2 line emission arise from shock-ionized stellar wind and entrained molecular clumps, respectively, while the HCO^+ emission arises from shock-compressed ambient cloud gas, this model predicts that the Hα and H_2 clumps should exhibit a greater velocity dispersion than the HCO^+ clumps, just as observed.

iii. *The Kelvin-Helmholtz jet model.*—In terms of the resulting morphology, this model displays a strong resemblance to model (ii), only, instead of a varying external pressure, the nonlinear growth of Kelvin-Helmholtz instabilities, stimulated as a result of differential flow between the jet material and the surrounding ambient medium, is the main process underlying the creation of the periodic pattern seen in shocked line emission (Blandford and Pringle 1976; Cohn 1983; Payne and Cohn 1985). The essence of this model is that the Kelvin-Helmholtz instability taps the relative kinetic energy between the jet and the ambient medium and converts it into sideways motion of the material near the interface. This lateral motion is manifested in the form of a series of incident-reflected shock pairs which propagated down the length of the jet. The points where the incident and reflected shocks are the regions of high pressure associated with the knots of shock-excited Hα and H_2 line emission. This situation is similar to that illustrated previously in Figure 11*b*. As is the case for model (ii), the regions of high compression are periodically placed along the jet axis, with a well-defined spacing (typically a few jet diameters) that depends on the Mach number of jet material, the ratio of internal to external pressures and the jet diameter (Payne and Cohn 1985; Garden *et al.* 1989*a*). However, there exists a fundamental difference between the pressure-confined and Kelvin-Helmholtz jet models being that in the first case the reflected shock pattern is stationary with respect to the surrounding ambient medium, while in the latter case the shock pattern (and thus the knots of shock-excited line emission) should move down the jet with a speed comparable to the jet material. If the source is sufficiently close (i.e., <1 kpc) then proper motion studies of the individual knots in a jet should provide an unambiguous test of these two models. Indeed, Herbig and Jones (1983) have already attempted such an observation and find that HH 7, 8, 9, and 10 are stationary but that HH 11, the innermost knot to the driving source, is moving outward with a tangential velocity of ~ 60 km s^{-1}. Note that this is in contrast to the radial velocity measurements of Solf and Bohm (1987), who measure a blueward shift in the radial velocity of up to ~ 60 km s^{-1} for HH 7, 8, and 10 and a significantly larger blueward shift of ~ 190 km s^{-1} for HH 11 relative to the cloud rest velocity. The existing observations are therefore ambiguous and cannot yet unequivocally distinguish between the two scenarios. Further observations aimed at measuring the proper motions of the shock-excited knots (both in optical and infrared lines) are clearly warranted.

To summarize, we tend to favor a hydrodynamic origin for the internal structure of the H_2 jets, mainly because periodic clumping is a natural product of hydrodynamic instabilities in a pressure-confined jet, which is not necessarily the case for the shocked cloudlet model.

iv) *A New Twin-Jet Source South of HH 7–11*

While observing the HH 7–11 source, we discovered a new H_2 emission-line source displaced approximately 3′ to the south of SSV 13. This position, which looked dark through the optical guide camera, was initially chosen as a sky frame (for flat-fielding purposes) but was found to contain bright H_2 $v = 1$–0 $S(1)$ line emission. Figure 12 (Plate 8) shows a mosaic of the entire region; further images obtained on a subsequent night failed to detect any strong continuum, thus indicating that most of the observed emission probably arises from H_2 lines. The shape of the H_2 source is unlike any we have seen before; taking the form of a "V" with a clumpy structure at its apex. It is tempting to suggest that the "V" shape is formed by two well-collimated jets that emanate from the same side of the clumpy source at its apex, which may be some variant of a young stellar object of T Tauri star. More detailed infrared spectroscopic observations are required in order to identify the nature of this source.

d) HH 12

HH 12 has already been found to be a source of H_2 line emission (Simon and Joyce 1983; Lane and Bally 1986). Our image of the H_2 $v = 1$–0 $S(1)$ line (+ continuum) emission is shown in Figure 13 (Plate 9) and a sketch of the image is shown in Figure 14. Again, the morphology is extremely clumpy and, as is the case for HH 7–11, there is a considerable resemblance of the H_2 line emission to the complex structure seen in optical Hα emission-line images (Strom *et al.* 1986). A high-velocity CO flow is also associated with HH 12 (Edwards and Snell 1983).

Although the bright, shock-excited Herbig-Haro objects appear to be associated with the SSV 12 source, proper motion studies in the optical have identified that they are moving to the north and are most probably excited by a different young stellar object that is located several arcmin to the south of SSV 12 (Strom, Strom, and Stoke 1983). The bright cone of emission that extends from SSV 12 to the west is also present in the continuum image and is thus most likely a reflection nebula that is illuminated by SSV 12. Beyond the outer edge of the cone-shaped reflection nebula, a narrow jet of weak H_2 line

PLATE 8

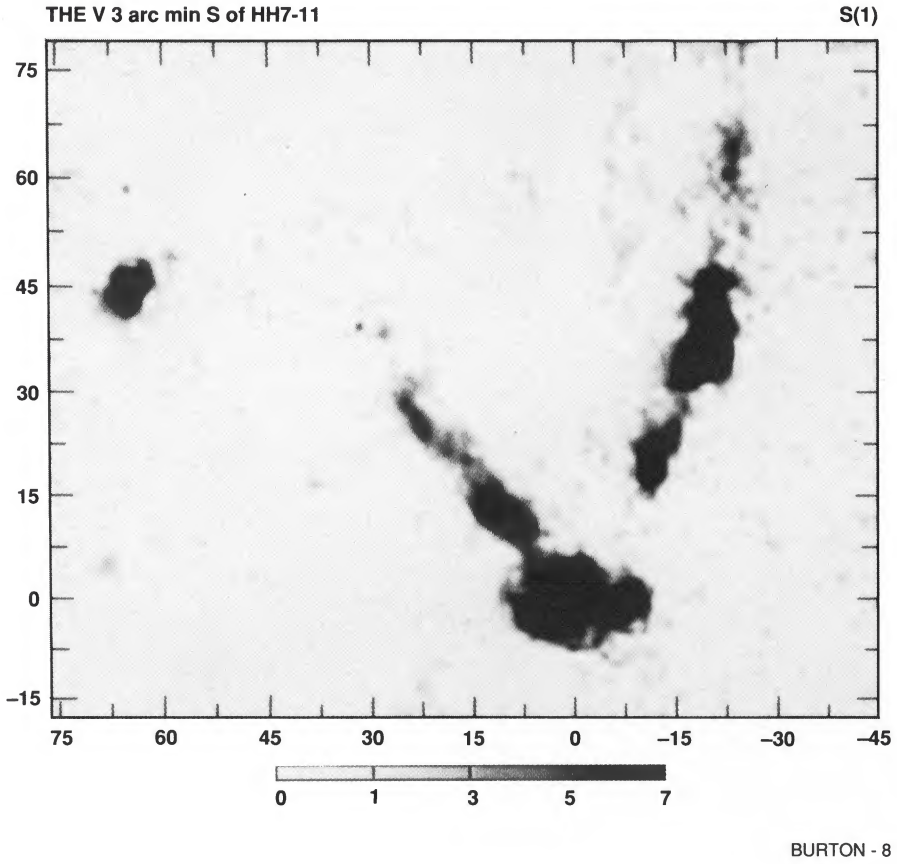

FIG. 12.—Image of H_2 $v = 1$–0 $S(1)$ (+ continuum) emission toward a newly discovered source located $\sim 3'$ to the south of HH 7–11, observed through a 1% resolution filter, with a plate scale of 1.2 arcsec per pixel. There is no continuum emission in this image. The gray scale at the bottom is in flux units of 10^{-23} W cm^{-2} arcsec^{-2}. The spatial offsets are in arcseconds, and the (0, 0) position is located at R.A. = $3^h26^m1\overset{s}{.}8$, Decl. = 31°02′10″ (this paper).

GARDEN *et al.* (*see* **354**, 239)

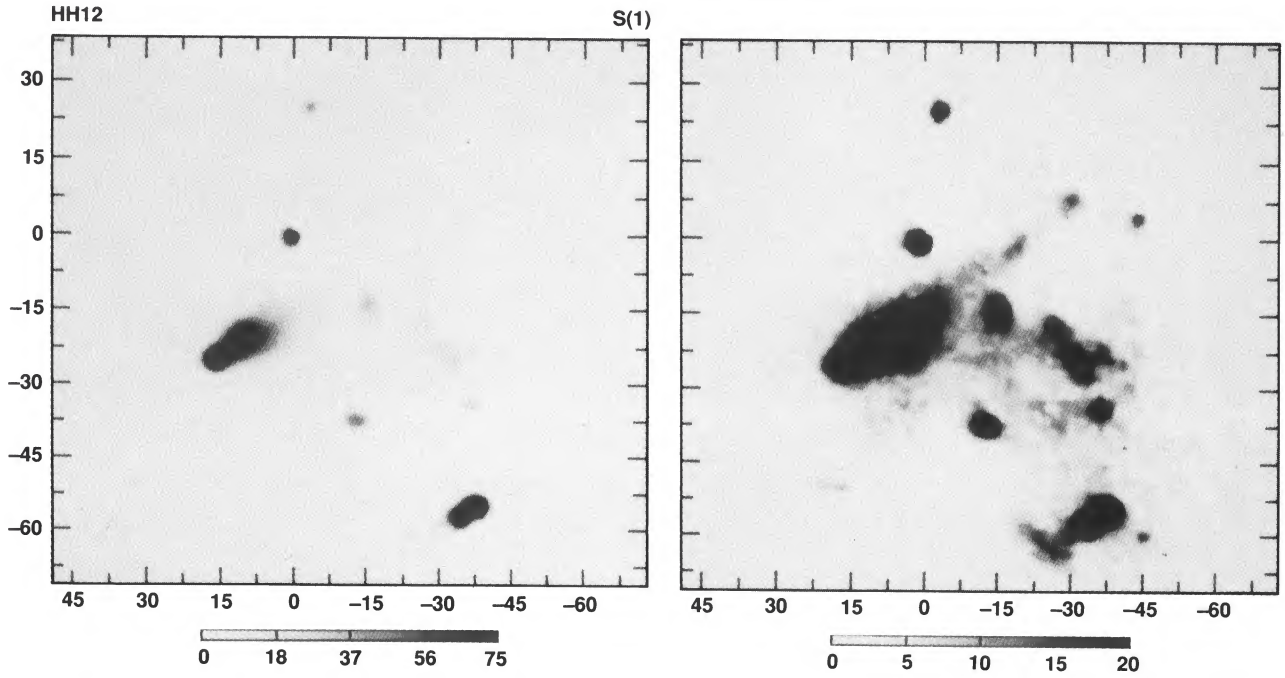

FIG. 13.—High and low contrast images of H_2 $v = 1$–0 $S(1)$ (+ continuum) emission in HH 12, observed through a 1% resolution filter, with a plate scale of 1.2 arcsec per pixel. Figure 11 provides further explanatory information. The gray-scale bar at the bottom of each image is in units of 10^{-23} W cm^{-2} arcsec^{-2}. The spatial offsets are in arcseconds, and the (0, 0) position is centered on star no. 18 (Herbig and Jones 1983) at R.A. = $3^h25^m54^s.7$, Decl. = 31°10′26″.7.

GARDEN *et al.* (*see* **354**, 239)

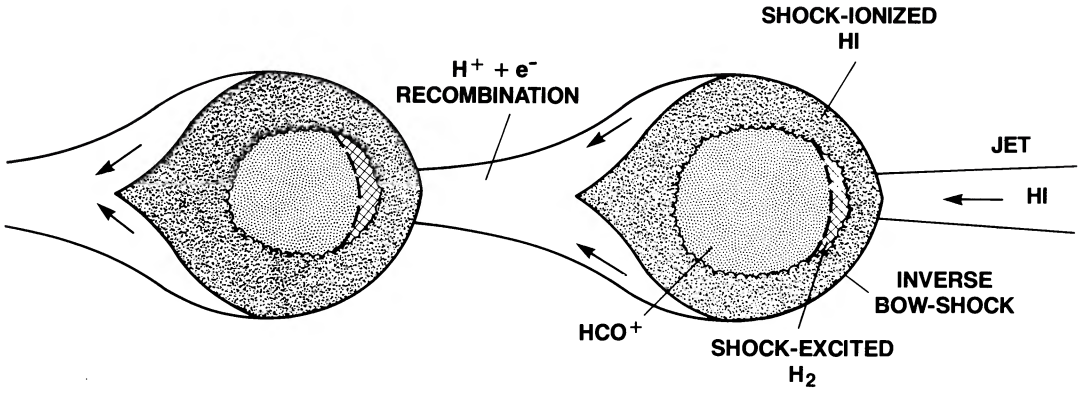

FIG. 11*a*

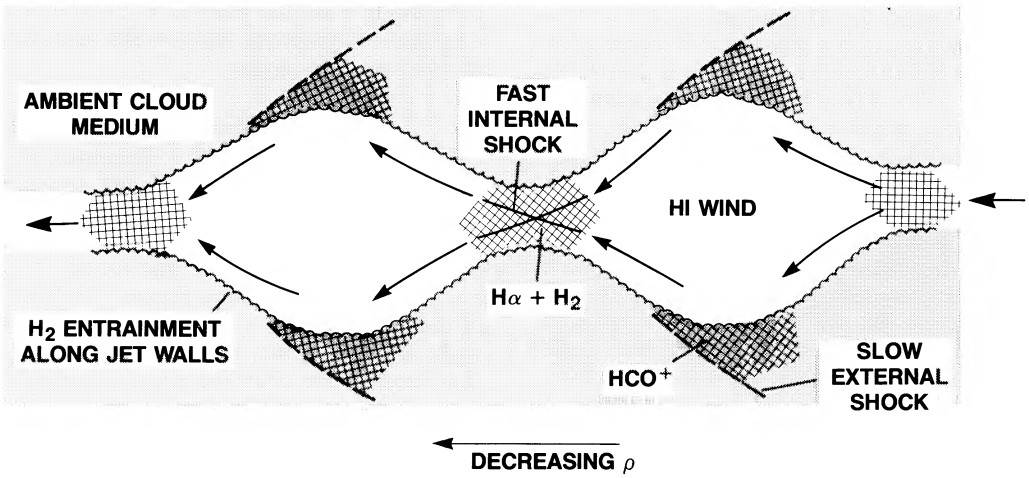

FIG. 11*b*

FIG. 11.—Schematic illustrations of (*a*) the shocked cloudlet model and (*b*) the pressure-confined jet model for the HH 7–11 and NGC 2071 sources

emission continues to propagate into the surrounding interstellar medium. As this thin jet appears to emanate from the immediate surroundings of SSV 12, it is most probable that SSV 12 may itself be a mass-loss object and that the reflection nebula may trace the outerwalls of a hollow cavity that has been swept out by a wind emanating from SSV 12.

IV. SUMMARY AND CONCLUSIONS

1. A common characteristic of the five outflow sources studied in this work is that they all possess collimated jets of shock-excited gas, which are extremely clumpy, often consisting of bright knots of hot gas that are placed periodically along the jet axis.

2. In the case of DR 21, and possibly also NGC 2071, the H_2 jets appear to become more collimated with increasing distance from the central driving source.

3. The hot shocked gas exists along the entire length of the jets; in the case of DR 21 it extends to several parsecs from the central driving source. This suggests that the jets are filled everywhere with supersonic turbulent motions that result in multiple shocks which heat the outflowing gas. Where the wind velocities are high enough to ionize the postshock gas, as in the case for the Herbig-Haro objects (HH 7–11 and HH 12), our H_2 line images appear to indicate that the ionized and hot molecular components are spatially coincident to within the limiting spatial resolution of the current observations (0.005 pc at a distance of 500 pc).

4. In general, the H_2 line emission in the DR 21, NGC 2071, and HH 7–11 outflow sources is well correlated with the distribution of CO emission, both exhibiting bipolar morphologies of comparable spatial extent. In all cases discussed here, the H_2 emission appears to be more collimated than the CO, presumably because of the higher angular resolution afforded by the infrared observations. For each of the outflow sources observed, the opposite lobes of the H_2 flows appear to differ significantly in spatial extent, degree of collimation, and brightness. These differences may result from a combination of extinction by foreground cloud material (especially in the case of the redshifted outflow lobes) and an inhomogeneous density distribution in the surrounding ambient cloud medium. Indeed, collisions with dense clumps of ambient cloud gas may deflect the jets, thereby accounting for some of the peculiar wiggles and sharp bends seen in the DR 21 and NGC 2071 H_2 *S*(1) line images.

5. The pressure confinement of a stellar wind which propagates through a dense, flattened cloud core or disk may explain the large-scale structure of the H_2 line emission seen toward the DR 21 and NGC 2071 star-forming regions. In the case of

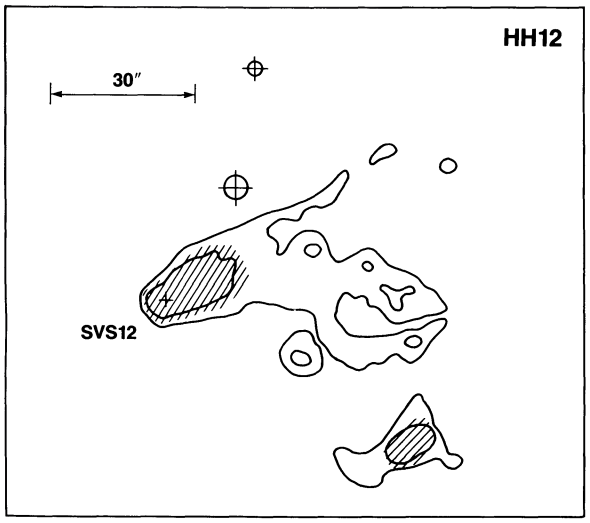

FIG. 14.—As for Fig. 3, schematic diagram of the H_2 $v = 1$–0 $S(1)$ line emission from HH 12 (see Fig. 12). The line-shaded area denotes a region of extended 2 μm continuum emission. The location of the IR source SSV 12 and the stars are shown with crosses.

HH 7–11, and maybe also DR 21 and NGC 2071, the collision of the wind with dense, preexisting clumps of gas in the ambient cloud medium, or the growth of Kelvin-Helmholtz instabilities along the walls of a pressure-confined jet, may help explain the complex internal morphology of the H_2 line emission.

6. We suggest that future observations should be aimed at measuring the velocity field of the hot shocked gas internal to the supersonic jets, and of the cooler ambient cloud gas that possibly confines the jets. Such observations are central to the development of our understanding of the physical nature of high-mass outflows and their influence on the surrounding ambient cloud medium.

We are grateful to Dolores Walther, Mark Casali, and Colin Aspin for support in operating IRCAM on UKIRT and to Bill Dent for allowing us to publish the JCMT data. R. P. G. acknowledges the support of the National Science Foundation through an NSF grant AST8513415 and an Alfred P. Sloan Fellowship. M. G. B. acknowledges the support of the National Research Council through an NRC NASA Research Associateship held at the NASA Ames Research Center.

REFERENCES

Bally, J. 1986, in *Masers, Molecules and Mass Outflows in Star Forming Regions*, proc. meeting held at Haystack Observatory, Westford, MA, USA on 1985 May 15–16, ed. A. P. Haschick.
Bally, J., and Predmore, C. R. 1983, *Ap. J.*, **265**, 778.
Blandford, R. D., and Pringle, J. E. 1976, *M.N.R.A.S.*, **176**, 443.
Buhrke, T., Mundt, R., and Ray, T. P. 1988, *Astr. Ap.*, **200**, 99.
Burton, M. G., Brand, P. W. J. L., Geballe, T. R., and Webster, A. 1989, *M.N.R.A.S.*, **236**, 409.
Burton, M. G., Geballe, T. R., and Brand, P. W. J. L. 1989, *M.N.R.A.S.*, **238**, 1513.
Burton, M. G., Geballe, T. R., Brand, P. W. J. L., and Webster, A. 1989, *M.N.R.A.S.*, **231**, 617.
Canto, J., Tenorio-Tagle, G., and Rozyczka, M. 1988, *Astr. Ap.*, **192**, 287.
Cohn, H., 1983, *Ap. J.*, **269**, 500.
Dickel, H. R., Goss, W. M., Rots, A. H., and Blout, H. M. 1986, *Astr. Ap.*, **120**, 74.
Edwards, S., and Snell, R. L. 1984, *Ap. J.*, **287**, 237.
Garden, R. P., Geballe, T. R., Gatley, I., and Nadeau, D. 1986, *M.N.R.A.S.*, **220**, 203.
———. 1989*a*, *Ap. J.*, submitted.
Garden, R. P., Gatley, I., Hayashi, M., and Hasegawa, T. 1989*b*, *Ap. J.*, submitted.
Gatley, I. 1988, in *Galactic and Extragalactic Star Formation*, ed. R. E. Pudritz and M. Fich (Dordrecht: Reidel), p. 159.
Grossman, E. N., Masson, C. R., Sargent, A. I., Scoville, N. Z., Scott, S., and Woody, D. P. 1987, *Ap. J.*, **320**, 356.
Harris, S. 1973, *M.N.R.A.S.*, **162**, 5 P.
Harvey, P. M., Marshall, J., Lester, D. F., and Wilking, B. A. 1986, *Ap. J.*, **360**, 737.
Herbig, G. H., and Jones, B. F. 1983, *A.J.*, **88**, 1040.
Hill, J. K., and Hollenbach, D. 1978, *Ap. J.*, **225**, 390.
Hollenbach, D., and McKee, C. F. 1989, *Ap. J.*, **342**, 306.
Königl, A. 1982, *Ap. J.*, **261**, 115.
Lane, A. P., and Bally, J. 1986, *Ap. J.*, **310**, 820.
Lane, A. P., Hass, M. R., Hollenbach, D. J., and Erickson, E. F. 1989, *Ap. J.*, submitted.
Lightfoot, J. F., and Glencross, W. M. 1986, *M.N.R.A.S.*, **221**, 993.
Lizano, S., Heiles, C., Rodriguez, L. F., Koo, B. C., Shu, F. H., Hasegawa, T., Hayashi, S., and Mirabel, I. F. 1988, *Ap. J.*, **328**, 763.
McLean, I. 1987, in *Proc. of the Workshop on Ground-based Astronomical Observations with Infrared Array Detectors*, ed. C. G. Wynn-Williams and E. Becklin (Honolulu: University of Hawaii), p. 180.
Mundt, R. 1984, in *Protostars and Planets II*, ed. D. Black and M. S. Mathews (Tucson: University of Arizona Press), p. 414.
———. 1988, in *Formation and Evolution of Low Mass Stars*, ed. A. K. Dupree and M. T. V. T. Largo (NATO ASI), in press.
Mundt, R., Brugel, E.W., and Buhrke, T. 1987, *Ap. J.*, **319**, 275.
Norman, M. L., Smarr, L., and Winkler, K. H. 1984, in *Numerical Astrophysics*, ed. J. Cantrella, J. LeBlanc, and R. Bowers (Boston: Jones & Bartlett), p. 88.
Payne, D. G., and Cohn, H. 1985, *Ap. J.*, **291**, 655.
Persson, S. E., Geballe, T. R., Simon, T., Lonsdale, C. J., and Baas, F. 1981, *Ap. J. (Letters)*, **251**, L85.
Righini-Cohen, G., Simon, M., and Young, E. T. 1979, *Ap. J.*, **232**, 782.
Roelfsema, P. R., Goss, W. M., and Geballe, T. R. 1989, preprint.
Rozyczka, M., and Tenorio-Tagle, G. 1985, *Astr. Ap.*, **147**, 209.
Rudolph, A., and Welch, W. J. 1988, *Ap. J. (Letters)*, **326**, L31.
Shull, J. M., and Beckwith, S. 1982, *Ann. Rev. Astr. Ap.*, **20**, 163.
Simon, T., and Joyce, R. R. 1983, *Ap. J.*, **265**, 864.
Snell, R. L., Scoville, N. Z., Sanders, D. B., and Erickson, N. R. 1984, *Ap. J.*, **284**, 176.
Solf, J., and Bohm, K. H. 1987, *A.J.*, **93**, 1172.
Strom, K. M., Strom, S. E. and Stocke, J., 1983, *Ap. J. (Letters)*, **271**, L23.
Strom, K. M., Strom, S. E., Wolff, S. C., Morgan, J. and Wenz, M. 1986, *Ap. J. Suppl.*, **62**, 39.
Tielens, A. G. G. M., and Hollenbach, D. 1985, *Ap. J.*, **291**, 722.
Wynn-Williams, C. G., and Becklin, E. E. 1987, *Proc. Workshop on Ground-based Astronomical Observations with Infrared Array Detectors* (Hilo). ed. C. G. Wynn-Williams and E. Becklin.
Zealey, W. J., Williams, P. M., and Sandell, G. 1984, *Astr. Ap.*, **140**, L31.
Zinnecker, H., Mundt, R., Geballe, T., and Zealy, W. J. 1989, preprint.

MICHAEL G. BURTON: NASA Ames, MS245-6, Moffett Field, CA 94035

ROGNVALD P. GARDEN: Department of Physics, University of California at Irvine, Irvine, CA 92717

ADRIAN P. G. RUSSELL: Joint Astronomy Center, 665 Komohana Street, Hilo, HI 96720